Modular Optical Cross-Connects (OXCs) for Large-Scale Optical Networks

Kui Chen, Tong Ye, Hao He, and Zidong Guo

***Abstract*— Due to the explosive growth of traffic demands, large-scale optical cross-connects (OXCs) are highly desired in next-generation optical networks. However, the scalability of classical OXCs is not good in terms of the size of optical switching modules and cabling complexity to meet application requirement. To address this issue, this letter proposes a two-phase approach to construct modular large-scale OXCs, using a set of small-size OXC modules. We first decompose each optical space switch (OS) in a classical OXC to a Clos network and then merge the corresponding links and decomposed optical switching modules of different Clos networks to form small-size OXC modules, which finally yields a modular OXC. We show that the proposed modular OXC has good scalability and acceptable physical-layer performance.**

***Index Terms*— Modularity, optical cross-connect (OXC), optical network.**

I. Introduction

OPTICAL cross-connect (OXC) based switching node is one of essential components in wavelength routing optical networks [1], [2]. With the explosive growth of traffic demands driven by high-bandwidth applications, the number of wavelength-division-multiplexing (WDM) fiber links between two adjacent switching nodes in the networks are being forced to increase fast due to the limitation of the capacity per link [2]–[4]. Therefore, large-scale OXCs are highly desired.

However, the scalability of classical OXCs is poor in terms of the size of each module and the number of fiber links. As Fig. 1 shows, an $N\times N$ OXC with w wavelength channels consists of w $N\times N$ optical space switches (OSs) sandwiched by N $1\times w$ input wavelength demulitplexers (DeMuxs) on the left and N $w\times 1$ wavelength multiplexers (Muxs) on the right. The OS is typically a micro-electro mechanical system (MEMS). Though free-space-optics based 3-D MEMSs with port count larger than 300 have been commercial, such kind of MEMSs is somewhat bulky for practical applications [5]–[7]. On the other hand, cabling complexity has been an important concern in the application of large-scale switching node [8]. In a classical OXC, there is one and only one fiber link between the optical components in two adjacent stages, and thus the number of fibers is $2Nw$. If we want to construct, for example, a 320×320 OXC with 24 wavelengths directly from 24 320×320 MEMSs, the number of fiber links will be 15360, which will impose a heavy maintenance burden on the network operators. Thus, as Ref. [7] pointed out, the construction of the OXC from large-scale MEMSs is not practical.

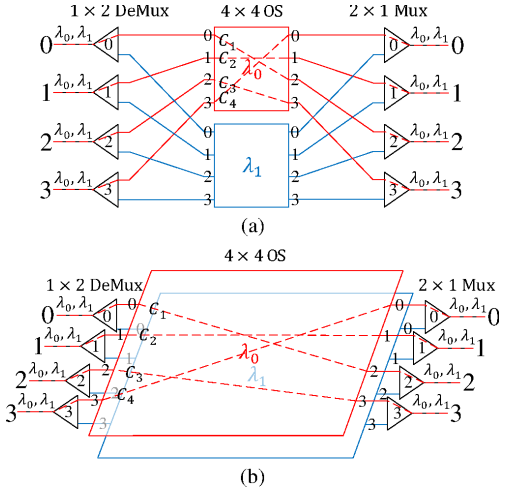

Fig. 1. A 4×4 OXC: (a) planar structure, and (b) stereo representation.

To address scalability issue, several kinds of large-scale OXCs have been proposed. Ref. [3] constructed a large-scale two-stage-routing OXC using a set of small-size wavelength selective switches (WSSs). However, such OXC cannot freely switch a wavelength from any input to any output due to the use of coarser-granular switching devices. In [4], a modular OXC was constructed from a set of small-scale OXCs connected in a ring topology. Such kind of OXC has two drawbacks. Firstly, its network structure is completely different from that of the classical OXCs and thus requires a different routing algorithm. This means the operation principle is not compatible with the classical OXCs. Secondly, the insertion loss of the OXC remarkably increases with the port count, which clearly limits the scalability.

In this letter, we propose a two-phase approach to construct a modular OXC, which is an interconnection network of small-size OXC modules. We start with a large-scale classical OXC. In phase 1, we decompose each OS in the OXC into a three-stage Clos network to modularize the OSs, which however doubles the number of interconnection links in the OXC. In phase 2, we merge the corresponding links and decomposed switching modules of different Clos networks to

Manuscript received November 20, 2018; revised February 28, 2019; accepted March 17, 2019. Date of publication March 22, 2019; date of current version May 7, 2019. This work was supported in part by the National Natural Science Fund of China under Grant 61671286, Grant 61571288, Grant 61433009, and Grant 61575123. *(Corresponding author: Tong Ye.)*

The authors are with the State Key Laboratory of Advanced Optical Communication Systems and Networks, Shanghai Jiao Tong University, Shanghai 200240, China (e-mail: aogutiancheng@sjtu.edu.cn; yetong@sjtu.edu.cn; hehao@sjtu.edu.cn; asunders@sjtu.edu.cn).

Color versions of one or more of the figures in this letter are available online at http://ieeexplore.ieee.org.

Digital Object Identifier 10.1109/LPT.2019.2907001

form a small-scale OXC module, such that the number of fiber links that interconnect the small-size OXC modules is reduced to $4N$. After such procedure, we transform a large-scale classical OXC to a modular OXC, which possesses the following advantages:

(1) It can be constructed from a set of small-size OXC modules, each of which is easy to synthesize and may even be integrated in a chip [9] in the near future;
(2) The number of fiber links that interconnect the OXC modules is only $2/w$ of that of the traditional OXC, which remarkably reduces the cabling complexity;
(3) It is non-blocking at each wavelength, and its routing algorithm is compatible with that for classical Clos networks;
(4) Its insertion loss is acceptable, and does not increase fast with the port count.

II. Construction Approach for Modular OXCs

To facilitate the presentation, we denote an $N\times N$ OXC, as $\mathcal{O}_A(N, w)$. For example, the OXC in Fig. 1(a) is an $\mathcal{O}_A(4, 2)$.

We number the DeMuxs by $0, 1, \cdots, N-1$, and the Muxs by $0, 1, \cdots, N-1$ from top to bottom. Each DeMux (or Mux) carries a wavelength set $\Lambda = \{\lambda_0, \lambda_1, \cdots, \lambda_{w-1}\}$. Similarly, we label the OSs by $0, 1, \cdots, w-1$. The lth OS performs switching for the signals at wavelength λ_l, where $l = 0, 1, \cdots, w-1$.

We denote a connection as $C(\alpha, \beta, \lambda_l)$, if it is a connection from wavelength λ_l at input α to that at output β, where $\alpha, \beta = 0, 1, \cdots, N-1$. The procedure that the OXC sets up connection $C(\alpha, \beta, \lambda_l)$ is as follows. At input α, the DeMux filters out λ_l from the input WDM signal and sends λ_l via its lth output to the αth input of OS l. Through reconfiguration, OS l can switch λ_l to the lth input of Mux β via its βth output. An example is $C_1(0, 2, \lambda_0)$ in Fig. 1.

This letter also refers to an OS in the classical OXC as a wavelength switching plane or a wavelength plane. To illustrate this concept, we represent the OXC in a stereo form, in which the DeMuxs/Muxs are respectively laid out from back to front, and the wavelength planes are stacked in parallel from top to bottom. As an example, Fig. 1(b) plots the stereo presentation of $\mathcal{O}_A(4, 2)$ in Fig. 1(a).

When N becomes large, the port count of each OS is large, and the scalability of classical OXCs is poor. In this section, we show how a large-scale OXC can be constructed from a set of small-scale OXC modules.

A. Decomposition

As Ref. [10] demonstrates, decomposition is a typical way for network modularization. We thus perform OS decomposition in the first step, to scale down the size of OSs in the OXC when N is large. In particular, we decompose each OS to a symmetric $N\times N$ three-stage Clos network, where there are:

(1) r $n\times n$ OSs in the first stage,
(2) n $r\times r$ OSs in the second stage,
(3) r $n\times n$ OSs in the third stage, and
(4) exactly one fiber link between the OSs at two adjacent stages, where $N = rn$.

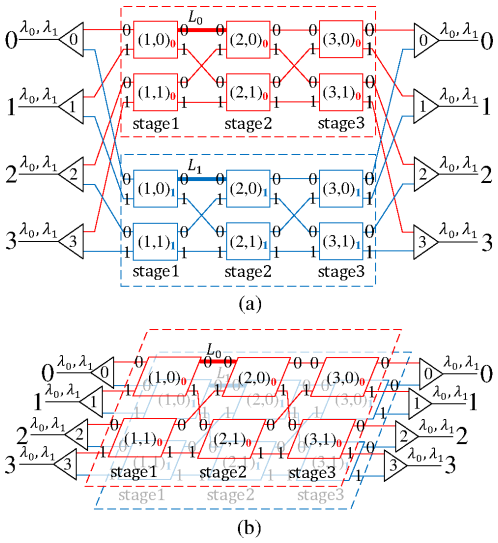

Fig. 2. A 4×4 network $\mathcal{O}_B(4, 2)$ after decomposition: (a) planar structure, and (b) stereo representation.

It is clear that each wavelength plane after the decomposition preserves the non-blocking property, according to the rearrangeably non-blocking condition of Clos networks.

After that, we obtain a switching network called $\mathcal{O}_B(N, w)$. For example, OXC $\mathcal{O}_A(4, 2)$ in Fig. 1(a) changes to $\mathcal{O}_B(4, 2)$ in Fig. 2(a), after each 4×4 OS or wavelength plane in Fig. 1(a) is decomposed to a 4×4 Clos network, in which $r = n = 2$. Accordingly, Fig. 2(b) is the stereo representation of Fig. 2(a).

Though the decomposition phase scales down the port count of each OS, it introduces $2Nw$ fiber links in additional, such that the number of fiber links that interconnect the network components is twice that of the original OXC. We thus need the second phase to reduce the number of fiber links.

B. Merge

At the lth wavelength plane, we denote an OS in $\mathcal{O}_B(N, w)$ as $(1, i)_l$ if it is the ith OS in the first stage, an OS as $(2, j)_l$ if it is the jth OS in the second stage, and an OS as $(3, k)_l$ if it is the kth OS in the third stage, where $i, k = 0, 1, \cdots, r-1$ and $j = 0, 1, \cdots, n-1$. For example, $(1, 1)_0$ is the 1st OS in the 1st stage at wavelength plan λ_0. Based on such numbering scheme, we can find that the stereo representation of $\mathcal{O}_B(N, w)$ has the properties as follows:

P1: OSs $(1, i)_0, (1, i)_1, \cdots, (1, i)_{w-1}$ are vertically aligned
OSs $(2, j)_0, (2, j)_1, \cdots, (2, j)_{w-1}$ are vertically aligned
OSs $(3, k)_0, (3, k)_1, \cdots, (3, k)_{w-1}$ are vertically aligned;
P2: Each $1\times w$ DeMux at the input side connects with a set of w vertically-aligned OSs at the first stage;
P3: Each $w\times 1$ Mux at the output side connects with a set of w vertically-aligned OSs at the third stage.

These properties hold since all the Clos networks at different wavelength planes have the same topology. For example, OS $(1, 0)_0$ and OS $(1, 0)_1$ in Fig. 2(b), are vertically aligned. This is also true for OS $(2, 0)_0$ and OS $(2, 0)_1$ in Fig. 2(b).

Fig. 3. Two vertically-aligned links can be implemented by a multi-fiber link containing two fibers.

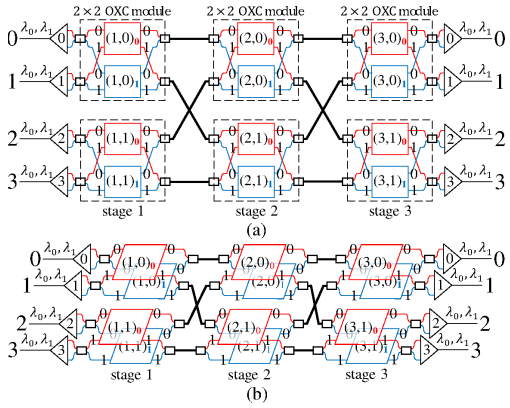

Fig. 4. A 4×4 modular OXC $\mathcal{O}_C(4,2)$: (a) planar structure, and (b) stereo representation.

Furthermore, 1×2 DeMux 3 connects with OSs $(1,1)_0$ and $(1,1)_1$, and 2×1 Mux 1 connects with OSs $(3,0)_0$ and $(3,0)_1$. It follows that w links between two sets of vertically-aligned OSs are also vertically aligned. For example, in Fig. 2, link L_0 between OS $(1,0)_0$ and OS $(2,0)_0$ is vertically aligned with link L_1 between OS $(1,0)_1$ and OS $(2,0)_1$.

Each set of w vertically-aligned links in $\mathcal{O}_B(N,w)$ can be implemented by a multi-fiber cable containing w fibers between two Multi-fiber PushOn (MPO) connecters. As Fig. 3 illustrates, the two links L_0 and L_1 in Fig. 2 can be implemented by a multi-fiber cable containing two fibers between a pair of MPO connecters. Note that, a currently commercial MPO connector only contains up to 24 fibers. Thus, if $w>24$, we need a bound of multi-fiber cables to replace a group of w vertically-aligned links. We expect that the number of fibers contained in an MPO connector could be large in the future.

We thus replace each set of w vertically-aligned links in $\mathcal{O}_B(N,w)$ by a multi-fiber cable, resulting in a new switching network called $\mathcal{O}_C(N,w)$. For example, $\mathcal{O}_C(4,2)$ in Fig. 4 is obtained by replacing each set of two vertically-aligned links in Fig. 2 by a multi-fiber cable.

According to P1 and P2, each set of w vertically-aligned OSs at the first stage is now sandwiched by n MPO connecters on the left and n MPO connecters on the right, which forms an $n\times n$ OXC module. In the same way, we obtain n $r\times r$ OXC modules at the second stage and r $n\times n$ modules at the third stage. We thus refer to $\mathcal{O}_C(N,w)$ as $N\times N$ modular OXC.

As Fig. 4 shows, the total number of links that interconnect the small-size OXC modules in modular OXC $\mathcal{O}_C(N,w)$ is $4N$, which is only $2/w$ of the number of the links that interconnect the OSs in the traditional OXC. Since the links inside each OXC module are encapsulated in a standard module, they do not increase the cabling complexity of the whole system. We thus claim that, compared with the classical OXC, the modular OXC reduces the cabling complexity by a fact of $w/2$. For example, we only need 1280 multi-fiber cables to construct a 320×320 modular OXC $\mathcal{O}_C(320,24)$.

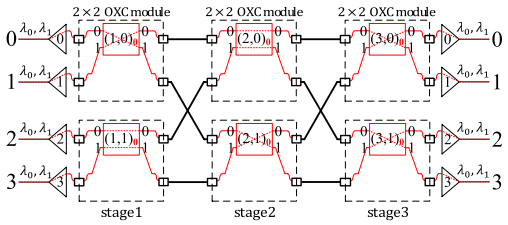

Fig. 5. Route assignments in the wavelength plane λ_0 of a modular OXC.

Also, there are N DeMuxs, N Muxs, $6N$ MPO connecters, $2rw$ $n\times n$ OSs, and nw $r\times r$ OSs in a modular OXC $\mathcal{O}_C(N,w)$. As an example, $\mathcal{O}_C(320,24)$ contains 320 DeMuxs, 320 Muxs, 1920 MPO connecters, 960 16×16 OSs, and 384 20×20 OSs.

III. Routing Process of Modular OXCs

In this section, we show how to assign routes for connection requests in modular OXC $\mathcal{O}_C(N,w)$. As we know, there is no wavelength converter in the modular OXC. It follows that, once the wavelength of a connection request is given, it can only pass through the OSs in the corresponding wavelength plane. Thus, the routing assignment of requests at different wavelengths can be coped with independently.

Suppose there are m requests $C_1, C_2, \cdots, C_m$ at wavelength λ_l, where $m\leq N$. We first ignore all the OSs at other wavelength planes. Clearly, the OSs at wavelength λ_l constitutes a Clos network, as Section II shows. For example, we want to assign routes for $C_1(0,2,\lambda_0)$, $C_2(1,1,\lambda_0)$, $C_3(2,3,\lambda_0)$, and $C_4(3,0,\lambda_0)$. We ignore the OSs at wavelength λ_1 and obtain a Clos network in Fig. 5.

The core issue of the routing in Clos network is to assign the OSs at the second stage to the requests. The routing constraint at each wavelength is that two requests cannot pass through the same OS at the second stage if they share the same OS at the first stage or the same OS at the third stage. Currently, there are a lot of classical algorithms available to solve the routing problem in Clos networks. For example, we can use the Karol′s algorithm in [11]. After such routing process, we can assign routes for C_1 through C_4, as Fig. 5 shows.

IV. Physical-Layer Performance

In this section, we carry out a proof-of-concept experiment to demonstrate that the proposed modular OXC is feasible in terms of physical-layer performance. We show that the end-to-end insertion loss of each connection is acceptable.

In our experiment, we take the 4×4 modular OXC in Fig. 4 as an example. We consider two connections C1 where all the 2×2 OSs are in bar state, and C2 where all the OSs are in cross state, to demonstrate the transmission performance difference of different connections.

Fig.6 plots the experimental setup. We first produce a 6-dBm 10-Gb/s optical signal via a 10-G directly modulated laser (DML) operating at 1550.54 nm, which is driven by a 10-Gb/s non-return-to-zero on-off-keying (NRZ-OOK) electrical signal generated by a pulse pattern generator (PPG, Anritsu MP1800A). We feed this optical signal to an optical connection, containing two 8×8 arrayed waveguide gratings (AWGs) and three 2×2 magneto-optical switches

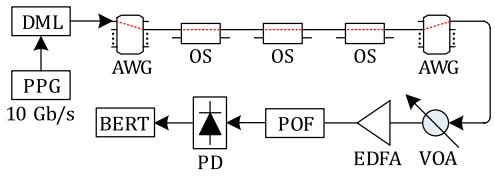

Fig. 6. Experimental setup.

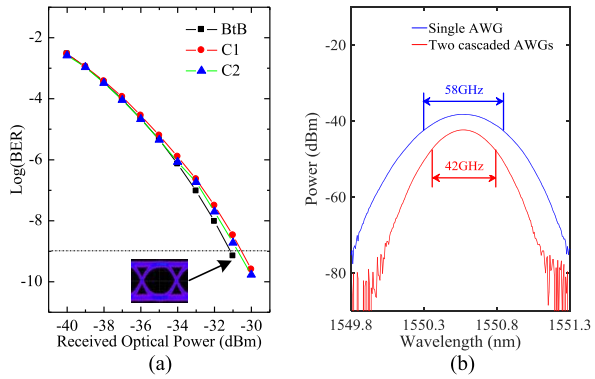

Fig. 7. Experimental results: (a) BER performance, and (b) pass band of two cascaded AWGs.

(Primanex MagLight^{TM}). Herein, we only use one input and two outputs of each 8×8 AWG to fulfill the function of a 1×2 DeMux (or 2×1 Mux). After the optical signal passes through C1 (or C2), the received optical power is −4.2 dBm (or −3.8 dBm). Thus, the insertion loss suffered by C1 (or C2) is 10.2 dB (or 9.8 dB).

At the receiver side, the optical signal in turn passes through a variable optical attenuator (VOA) for received optical power adjustment, an erbium-doped fiber amplifier (EDFA) for power amplification, and a programmable optical filter (POF, Finisar Waveshaper) for amplified spontaneous emission noise elimination. The electrical signal is retrieved from the optical signal by a photodiode (PD), and finally captured by a bit-error rate tester (BERT) to measure the bit-error-ratio (BER). In the transmission performance measurement, we consider the following two conditions:

(1) Back-to-back (BtB): the optical signal passes through a fiber link;
(2) C1/C2: the optical signal goes through C1/C2.

Experimental results are plotted in Fig. 7. It can be seen from Fig. 7(a) that the BER curves of the NRZ-OOK signals in C1 and C2 are almost the same, which demonstrates that the transmission performance difference of various connections is ignorable if the magneto-optical switch is used. Fig. 7(a) also shows that the power penalty of C1 is only 0.6 dB compared to BtB at BER $= 10^{-9}$, which is mainly attributed to the fact that the central frequency of the optical signal is drifted by the DML chirp, and the optical signal suffers from filtering effect [12] when it passes through two AWGs. As Fig. 7 (b) shows, the pass band of a single 100-GHz AWG is 58 GHz, and that of two cascaded 100-GHz AWG reduces to 42 GHz. From the result in Fig. 7, we conclude that the proposed modular OXC is feasible in terms of physical-layer performance.

The proposed $N \times N$ modular OXC has a good scalability in terms of optical insertion loss even when the port count N is large. In the modular OXC, each connection passes through 1 DeMux, 6 MPO connecters, 3 OSs, and 1 Mux. Compared with that in the classical OXC, each connection in the modular OXC traverses 6 more MPO connecters and 2 more OSs. The maximum insertion losses of a 100-GHz AWG-based Mux (or DeMux), an MPO connecter, and a 32-port OS are 5.5 dB [13], 0.35 dB, and 1.4 dB [14], respectively. Therefore, the worst-case insertion loss of a connection in the modular OXC is 17.3 dB, about 4.9 dB more than that in the classical OXC. If the modular OXC is deployed in optical networks, an EDFA will be needed at each output, which may be the cost of modularization. Even so, the modular OXC has an advantage that its insertion loss does not increase fast with the port count.

V. Conclusion

This letter proposes an approach to design modular OXCs, which possess the following advantages. First, it is constructed from a set of small-scale OXC modules, each of which is easy to synthesize and may even be integrated in a chip in the near future. Second, the number of fiber links that interconnect the OXC modules is only $2/w$ of that of the classical OXC. Third, it is non-blocking at each wavelength, and the routing algorithm is compatible with that for classical Clos networks. Furthermore, its insertion loss is acceptable, and does not increase fast with the port count.

References

[1] S.-K. Liaw, P.-S. Tsai, H. Wang, H. L. Minh, and Z. Ghassemlooy, "FBG-based reconfigurable bidirectional OXC for 8 × 10 Gb/s DWDM transmission," *Opt. Commun.*, vol. 358, pp. 154–159, Jan. 2016.
[2] J. Wu, S. Subramaniam, and H. Hasegawa, "Comparison of OXC node architectures for WDM and flex-grid optical networks," in *Proc. IEEE ICCCN*, Aug. 2015, pp. 1–8.
[3] H.-C. Le, H. Hasegawa, and K.-I. Sato, "Performance evaluation of large-scale multi-stage hetero-granular optical cross-connects," *Opt. Express*, vol. 22, no. 3, pp. 3157–3168, 2014.
[4] Y. Iwai, H. Hasegawa, and K.-I. Sato, "Large-scale photonic node architecture that utilizes interconnected small scale optical cross-connect sub-systems," in *Proc. ECOC*, 2012, pp. 1–3.
[5] Q. Cheng, S. Rumley, M. Bahadori, and K. Bergman, "Photonic switching in high performance datacenters [invited]," *Opt. Express*, vol. 26, no. 12, pp. 16022–16043, 2018.
[6] *S Series Optical Circuit Switch*. Accessed: 2019. [Online]. Available: https://www.calient.net/products/s-series-photonic-switch
[7] T. Ban, H. Hasegawa, K.-I. Sato, T. Watanabe, and H. Takahashi, "A novel large-scale OXC architecture and an experimental system that utilizes wavelength path switching and fiber selection," *Opt. Express*, vol. 21, no. 1, pp. 469–477, 2013.
[8] *Optical Networking in the Cloud and 5G Era*. Accessed: 2018. [Online]. Available: https://www.ofcconference.org/zh-cn/home/news-and-press/ofc-video-library
[9] S. Han, T. J. Seok, K. Yu, N. Quack, R. S. Müller, and M. C. Wu, "50 × 50 polarization-insensitive silicon photonic MEMS switches: Design and experiment," in *Proc. ECOC*, 2016, pp. 1–3.
[10] G. Maier, A. Pattavina, and S. G. Colombo, "Control of non-filterable crosstalk in optical-cross-connect Banyan architectures," in *Proc. IEEE GLOBECOM*, vol. 2, Nov./Dec. 2000, pp. 1228–1232.
[11] M. J. Karol and C.-C. I, "Performance analysis of a growable architecture for broad-band packet (ATM) switching," *IEEE Trans. Commun.*, vol. 40, no. 2, pp. 431–439, Feb. 1992.
[12] B.-H. Choi and S. S. Lee, "The effect of AWG-filtering on a bidirectional WDM-PON link with spectrum-sliced signals and wavelength-reused signals," *Opt. Commun.*, vol. 284, no. 24, pp. 5692–5696, 2011.
[13] *AWG Multi/Demultiplexer*. Accessed: 2019. [Online]. Available: http://www.ntt-electronics.com/en/products/photonics/awg_mul_d.html
[14] *Single Mode Optical Switches with up to 32 × 32 Ports*. Accessed: 2009. [Online]. Available: http://www.jencotech.com/documents/products/Series1000_Polatis_Data.pdf